Thermophoretic force on nonspherical particles in the free-molecule regime

Song Yu, Jun Wang,* Guodong Xia, and Luxiang Zong

Key Laboratory of Enhanced Heat Transfer and Energy Conservation, Ministry of Education, and Key Laboratory of Heat Transfer and Energy Conversion, Beijing Municipality, College of Environmental and Energy Engineering, Beijing University of Technology, Beijing 100124, People's Republic of China

(Received 9 February 2018; revised manuscript received 5 April 2018; published 17 May 2018)

The present paper is devoted to studying the thermophoresis of a nonspherical convex particle suspended in a gas with nonuniform temperature distribution in the free-molecule regime. Based on the gas kinetic theory and the assumption of a rigid-body collision for the gas-particle interaction, analytical expressions for the thermophoretic forces are obtained for several typical nonspherical bodies, including cylinders, spheroids, needles, disks, and cuboids. The orientation dependences of the thermophoretic forces and thermophoretic velocities are evaluated based on these expressions. It is found that the influence of the pitching effect of the nonspheres can be significant. The expressions for the orientation-averaged thermophoretic forces are also obtained under the assumption of a uniform particle orientation distribution.

DOI: 10.1103/PhysRevE.97.053106

I. INTRODUCTION

Thermophoresis describes the particle motion caused by a nonuniform temperature distribution in the surrounding fluid (usually a gas) [1–4]. The gas molecules with higher kinetic energy in the hot region usually impinge on the particle with greater momenta than those coming from the cold region, which results in a net force (thermophoretic force) in the direction from the hot to the cold side, as well as a drag opposite to the particle movement direction. The thermophoretic velocity of the particle is usually defined as the terminal velocity induced by the balance between the thermophoretic and drag forces. The thermophoresis phenomenon has been widely studied over the past decades, because it can find applications in numerous practical applications, including aerosol science [5,6], manufacturing of microelectronics [7–10], nuclear reactor safety [11], and combustion [12–16]. However, the underlying physics of thermophoresis is far from clear, not only for the evaluation of the thermophoretic force but also for its direction (negative thermophoresis is reported under some particular conditions) [17–24].

Theoretically, the thermophoretic force can be considered as the net momentum transfer from the gas molecules over the entire particle surface in unit time. The challenge is to obtain the molecule velocity distribution of a gas with nonuniform temperature distribution, which might be influenced by the presence of the particle. This difficulty could be greatly reduced in the free-molecule regime, where the Knudsen number $\mathrm{Kn} \gg 1$. Here, $\mathrm{Kn} = \lambda/L_c$, λ is the mean free path of the gas, and L_c is the characteristic size of the particle. In the free-molecule regime, the gas molecules reflected by the particle surface can usually move for a long distance before colliding with other gas molecules; i.e., the interactions between the incident gas molecules and those reflected by the particle surface can be neglected. Therefore, the macroscopic motion of the gas induced by the presence of the particle is also neglected. Therefore, it is reasonable to assume that the gas molecule velocity distribution is uninfluenced by the particle. In the continuum ($\mathrm{Kn} \ll 1$) and transition ($\mathrm{Kn} \sim 1$) regimes, the influence of the particle on the molecule velocity distribution of the gas cannot be neglected, and there exist several analytical approaches based on different approximation methods for the Boltzmann transport equation [25–31]. However, the validity of these approaches still remains debatable [32,33].

In the free-molecule regime, based on the gas kinetic theory [34,35], Waldmann [36] determined the thermophoretic force on a spherical particle suspended in a gas under the assumption of rigid-body collisions between the gas molecules and the particle. The Waldmann equation for the thermophoretic force is given by [36]

$$\mathbf{F}_T = -\frac{8\kappa}{15}\sqrt{\frac{2\pi m}{k_B T}}R_0^2 \nabla T, \tag{1}$$

where, κ is the thermal conductivity of the gas, m is the gas molecule mass, k_B is the Boltzmann constant, T is the gas temperature, R_0 is the radius of the spherical particle, and ∇T is the temperature gradient of the gas (here, the positive direction of ∇T is from the cold to the hot side). It is clearly seen that the thermophoretic force is in the direction opposite to the temperature gradient, i.e., from the hot to the cold side. Experimental [37–43] and numerical [29,44] studies have shown that the Waldmann equation predicts the thermophoretic forces quite well for larger Knudsen numbers. However, negative thermophoresis (thermophoretic force is from low to high temperature) becomes possible as the particle size decreases from micro- to nanoscale [21]. Moreover, negative thermophoresis can also be observed as the flow regime is in the continuum regime, when the particle has a thermal conductivity much higher than that of the surrounding fluid [23].

*jwang@bjut.edu.cn

It should be noted that the majority of the previous investigations on thermophoresis are for spheres, even though most aerosol particles of practical interest are definitely nonspheres. It is a general and convenient theoretical method to simplify a real particle into a sphere. However, the effect of the particle shape and orientation on its transport is reported to be significant according to the available literature [45–61]. In the free-molecule regime, Garcia-Ybarra and Rosner [45] analyzed the thermophoresis of a spherocylinder (a cylinder with two hemispherical caps at both ends) and evaluated the thermophoretic force on the cylinder particle. The thermophoretic force on the cylindrical part is given by [45]

$$\mathbf{F}_T = -\frac{\kappa}{5}\sqrt{\frac{2\pi m}{k_B T}} R_0 L\left[\sigma \nabla T_{\parallel} + \left(2 - \frac{\sigma}{2}\right)\nabla T_{\perp}\right], \quad (2)$$

where R_0 is the cylinder radius; L is the cylinder length; the subscripts "$\perp$" and "$\parallel$" indicate the temperature gradient components perpendicular and parallel to the cylinder axis, respectively; and σ is the momentum accommodation coefficient. It is found that the thermophoretic velocity of the spherocylindrical particle with its axis aligned with ∇T is higher than that of a sphere with radius R_0 by about 31%, and the direction of the thermophoretic velocity can deviate from ∇T by an angle of 12° [45]. As for other nonspherical particles, few theoretical studies on thermophoresis are available in the free-molecule regime.

This paper is devoted to derive the expressions for the thermophoretic forces on the nonspherical particles of convex shapes in the free-molecule regime. The rest of the paper is organized as follows. In Sec. II, the molecule velocity distribution of a gas with a nonuniform temperature distribution is given based on the Chapman-Enskog thoery. In Sec. III, the explicit expressions for the thermophoretic forces on several typical nonspherical bodies, including cylinders, spheroids, needles, disks, and cuboids, are obtained on the basis of the gas kinetic theory. Finally, we conclude our paper in Sec. IV.

II. GAS MOLECULE VELOCITY DISTRIBUTION FUNCTION

As mentioned in Sec. I, in the free-molecule regime, the gas molecule velocity distribution is uninfluenced by the presence of the particle. According to the Chapman-Enskog theory [34,35], for a gas with nonuniform temperature distribution, the gas molecule velocity distribution reads

$$f = f_0(1 + \Phi), \quad (3)$$

where f_0 is the equilibrium Maxwellian velocity distribution function,

$$f_0 = n\left(\frac{h}{\sqrt{\pi}}\right)^3 \exp(-h^2 C'^2), \quad (4)$$

and Φ is the correction owing to the temperature gradient,

$$\Phi = -\frac{8h^4\kappa}{5\rho}\left(h^2 C'^2 - \frac{5}{2}\right)\mathbf{C}' \cdot \nabla T. \quad (5)$$

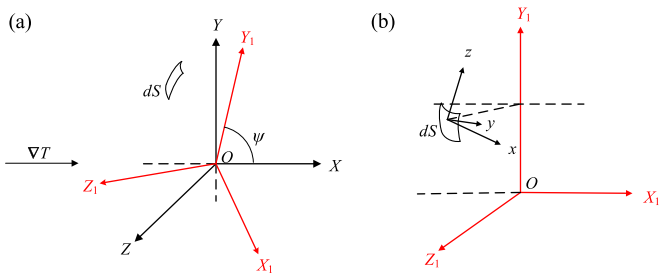

FIG. 1. The coordinate systems for a nonspherical particle suspended in a nonuniform temperature field of a highly rarefied gas.

Here, $h = \sqrt{m/(2k_B T)}$, n is the molecular number density of the gas, and $\mathbf{C}'$ is the thermal velocity of the gas molecule.

Consider a nonspherical particle with arbitrary convex surface suspended in a gas with nonuniform temperature field. A global coordinate system $\{X, Y, Z\}$ with its origin located at the center of the particle is established, as shown in Fig. 1(a), wherein X is in the direction of the temperature gradient. Let $\mathbf{I}$, $\mathbf{J}$, and $\mathbf{K}$ be the unit vectors in the X, Y, and Z directions, respectively. The thermal velocity of the gas molecule is $\mathbf{C}' = U'\mathbf{I} + V'\mathbf{J} + W'\mathbf{K} = (U', V', W')^{\mathrm{T}}$, and the temperature gradient is $\nabla T = (\nabla T, 0, 0)^{\mathrm{T}}$. A local coordinate system $\{x, y, z\}$ with its origin fixed to the surface element dS of the particle is also introduced, as shown in Fig. 1(b), wherein y is in the inward normal direction of dS, and x and z are tangent to dS. Let $\mathbf{i}$, $\mathbf{j}$, and $\mathbf{k}$ be the unit vectors in the x, y, and z directions, respectively. In the system $\{x, y, z\}$, the thermal velocity of the gas molecule is $\mathbf{c}' = u'\mathbf{i} + v'\mathbf{j} + w'\mathbf{k} = (u', v', w')^{\mathrm{T}}$. Then, the transformation between the above two coordinate systems can be expressed as

$$\mathbf{x} = \mathbf{M} \cdot \mathbf{X}, \quad (6)$$

where $\mathbf{x} = (x, y, z)^{\mathrm{T}}$, $\mathbf{X} = (X, Y, Z)^{\mathrm{T}}$, and the transformation matrix

$$\mathbf{M} = \begin{bmatrix} \alpha_X & \alpha_Y & \alpha_Z \\ \beta_X & \beta_Y & \beta_Z \\ \gamma_X & \gamma_Y & \gamma_Z \end{bmatrix}. \quad (7)$$

Here, Λ_X, Λ_Y, and $\Lambda_Z (\Lambda = \alpha, \beta, \gamma)$ are the direction cosines of $\mathbf{I}$, $\mathbf{J}$, and $\mathbf{K}$ in the coordinate system $\{x, y, z\}$, respectively.

According to the above definitions, the thermal velocity components in the global coordinate system can be expressed by those in the local coordinate system, $U' = u'\alpha_X + v'\beta_X + w'\gamma_X$, $V' = u'\alpha_Y + v'\beta_Y + w'\gamma_Y$, and $W' = u'\alpha_Z + v'\beta_Z + w'\gamma_Z$. Thus, the gas molecule velocity distribution function can be rewritten as

$$f = f_0\{1 + A\nabla T[h^2(u'^2 + v'^2 + w'^2) - \tfrac{5}{2}] \times (u'\alpha_X + v'\beta_X + w'\gamma_X)\}, \quad (8)$$

where the Maxwellian velocity distribution function f_0 is

$$f_0 = n\left(\frac{h}{\sqrt{\pi}}\right)^3 \exp[-h^2(u'^2 + v'^2 + w'^2)], \quad (9)$$

and $A = -8h^4\kappa/(5\rho)$.

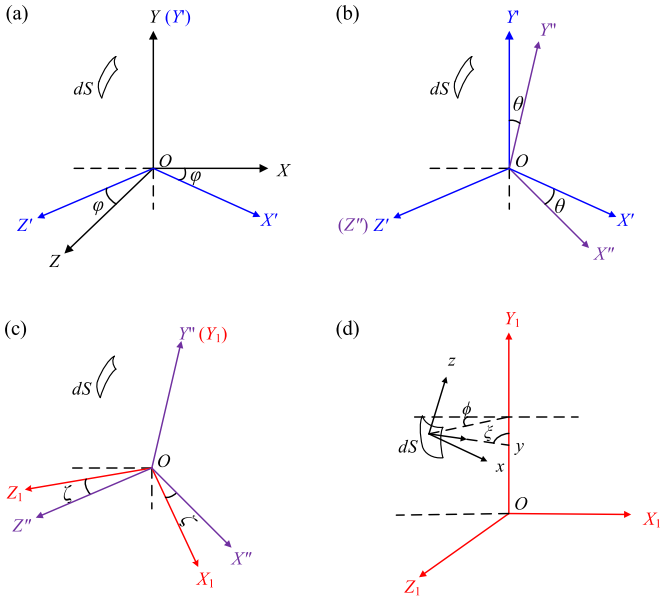

FIG. 2. The transformation between the global and local coordinate systems: (a)–(c) the global and auxiliary coordinate systems; (d) the auxiliary and local coordinate systems.

III. ANALYTICAL EXPRESSIONS FOR THERMOPHORETIC FORCES ON THE NONSPHERICAL PARTICLES

A. General integral expressions for the thermophoretic forces on rigid particles in the free-molecule regime

Based on the gas kinetic theory, the thermophoretic force can be considered as the net momentum transfer from the gas molecules over the entire particle surface in unit time, which consists of two contributions: momentum exchange due to the incident gas molecules and reflected ones [62–64]. In the present paper, we assume that the mass of the particle is much larger than that of the gas molecule. The net momentum transfer of the incident gas molecules can be calculated by an integration of the momentum transfer on the surface element, which depends on the velocity distribution function given by Eq. (8). The contribution by the reflected gas molecules depends on the reflection scenarios of the gas molecules upon collisions with the particle. There are two limiting cases of reflection: specular and diffuse reflections. For the specular reflection, the collision between the gas molecule and the particle is elastic and there is no tangential momentum transfer. For the diffuse reflection, the incident gas molecule is reemitted with an equilibrium Maxwellian distribution specified at the particle surface temperature T_w (assumed to be equal to the gas temperature T). Usually, the reflection is a mixing of specular and diffuse scatterings. It is conventional to introduce a momentum accommodation coefficient, which denotes the fraction of molecules reflected in a diffuse manner.

In the local coordinate system, the force on the surface element of the particle in the y direction is given by

$$p = p_i + p_r = (2 - \sigma_p)p_i + \sigma_p p_w, \tag{10}$$

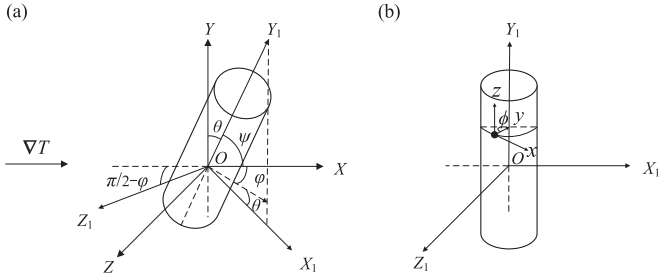

FIG. 3. The coordinate systems for a cylinder.

and the tangential forces in the x and z directions are

$$\tau_x = \tau_{xi} - \tau_{xr} = \sigma_\tau \tau_{xi}, \tag{11}$$

$$\tau_z = \tau_{zi} - \tau_{zr} = \sigma_\tau \tau_{zi}. \tag{12}$$

Here, p_i, τ_{xi}, and τ_{zi} are the normal and tangential forces induced by the impinging gas molecules, while p_r, τ_{xr}, and τ_{zr} are attributed to the reflection of the gas molecules. $\sigma_p = (p_i - p_r)/(p_i - p_w)$ and $\sigma_\tau = (\tau_i - \tau_r)/(\tau_i - \tau_w)$ are the normal and tangential momentum accommodation coefficients. p_w and τ_w are the normal and tangential forces due to the diffusely reflected gas molecules. Clearly, $\tau_w = 0$ and

$$\frac{p_w}{N_w} = \frac{\int_{-\infty}^{+\infty}\int_{-\infty}^{0}\int_{-\infty}^{+\infty} mv^2 f_0 du dv dw}{\int_{-\infty}^{+\infty}\int_{-\infty}^{0}\int_{-\infty}^{+\infty} (-v) f_0 du dv dw} = \frac{m\sqrt{\pi}}{2h}, \tag{13}$$

where N_w is the number of the diffusely reflected gas molecules. For completely diffuse reflection, N_w is equal to the total number of the impinging gas molecules N_i,

$$N_i = \int_{-\infty}^{+\infty}\int_{0}^{+\infty}\int_{-\infty}^{+\infty} vf du dv dw. \tag{14}$$

Then, the normal and tangential forces due to the impinging and outgoing gas molecules are expressed by

$$p_i = \int_{-\infty}^{+\infty}\int_{0}^{+\infty}\int_{-\infty}^{+\infty} mv^2 f du dv dw, \tag{15}$$

$$\tau_{xi} = \int_{-\infty}^{+\infty}\int_{0}^{+\infty}\int_{-\infty}^{+\infty} muvf du dv dw, \tag{16}$$

$$\tau_{zi} = \int_{-\infty}^{+\infty}\int_{0}^{+\infty}\int_{-\infty}^{+\infty} mvwf du dv dw, \tag{17}$$

$$p_w = \frac{m\sqrt{\pi}}{2h}\int_{-\infty}^{+\infty}\int_{0}^{+\infty}\int_{-\infty}^{+\infty} vf du dv dw. \tag{18}$$

By substituting Eqs. (8) and (9) into Eqs. (15)–(18), the parts of normal and tangential thermophoretic forces on the surface element are rewritten as

$$p_i = \frac{\rho A \nabla T \beta_X}{4\sqrt{\pi}h^3}\exp\left(-h^2 v_0^2\right), \tag{19}$$

$$\tau_{xi} = \frac{\rho A \nabla T}{8\sqrt{\pi}h^3}(\alpha_X - 2\beta_X h^2 u_0 v_0)\exp\left(-h^2 v_0^2\right), \tag{20}$$

$$\tau_{zi} = \frac{\rho A \nabla T}{8\sqrt{\pi}h^3}(\gamma_X - 2\beta_X h^2 w_0 v_0)\exp\left(-h^2 v_0^2\right), \tag{21}$$

$$p_w = -\frac{\rho A \nabla T \beta_X v_0}{8h^2}\exp\left(-h^2 v_0^2\right), \tag{22}$$

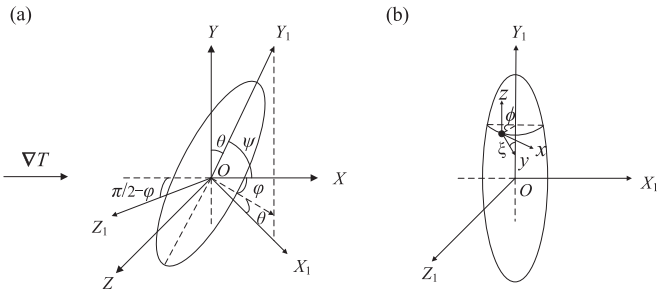

FIG. 4. The coordinate systems for a spheroid.

where u_0, v_0, and w_0 are the mass velocity components of the gas in the local coordinate system. Here, we focus our attention on subsonic gas flow, in which only the first order term of hv_0 is taken into account and the influence of higher order terms can be neglected. Finally, the thermophoretic force acting on the particle can be obtained by integrating the elementary force components (p, τ_x, and τ_z) over the whole surface of the particle,

$$F_X = \int_S \{\sigma_\tau \tau_{xi}\alpha_X + [(2-\sigma_p)p_i + \sigma_p p_w]\beta_X + \sigma_\tau \tau_{zi}\gamma_X\} dS, \tag{23}$$

$$F_Y = \int_S \{\sigma_\tau \tau_{xi}\alpha_Y + [(2-\sigma_p)p_i + \sigma_p p_w]\beta_Y + \sigma_\tau \tau_{zi}\gamma_Y\} dS, \tag{24}$$

$$F_Z = \int_S \{\sigma_\tau \tau_{xi}\alpha_Z + [(2-\sigma_p)p_i + \sigma_p p_w]\beta_Z + \sigma_\tau \tau_{zi}\gamma_Z\} dS, \tag{25}$$

which are expressed in the global coordinate system. Equations (23)–(25) could be considered as the general integral expressions for the thermophoretic forces on rigid nonspherical particles with a convex surface in the free-molecule regime. Note that the above derivation is restricted to the particle with a convex surface; otherwise multiple collisions should be taken into account.

B. Transformation matrices

Considering the influence of the particle's orientation on the thermophoresis, it is necessary to specify the orientation of the particle. An auxiliary coordinate system $\{X_1, Y_1, Z_1\}$ has to be introduced with its origin also fixed at the center of the particle as show in Figs. 1 and 2. Let $\mathbf{I}_1$, $\mathbf{J}_1$, and $\mathbf{K}_1$ be the unit vectors in the X_1, Y_1, and Z_1 directions, respectively. The coordinate system $\{X_1, Y_1, Z_1\}$ are related to coordinate systems $\{x, y, z\}$ and $\{X, Y, Z\}$ by

$$\mathbf{x} = \mathbf{M}_1 \cdot \mathbf{X}_1, \tag{26}$$

and

$$\mathbf{X}_1 = \mathbf{M}_2 \cdot \mathbf{X}, \tag{27}$$

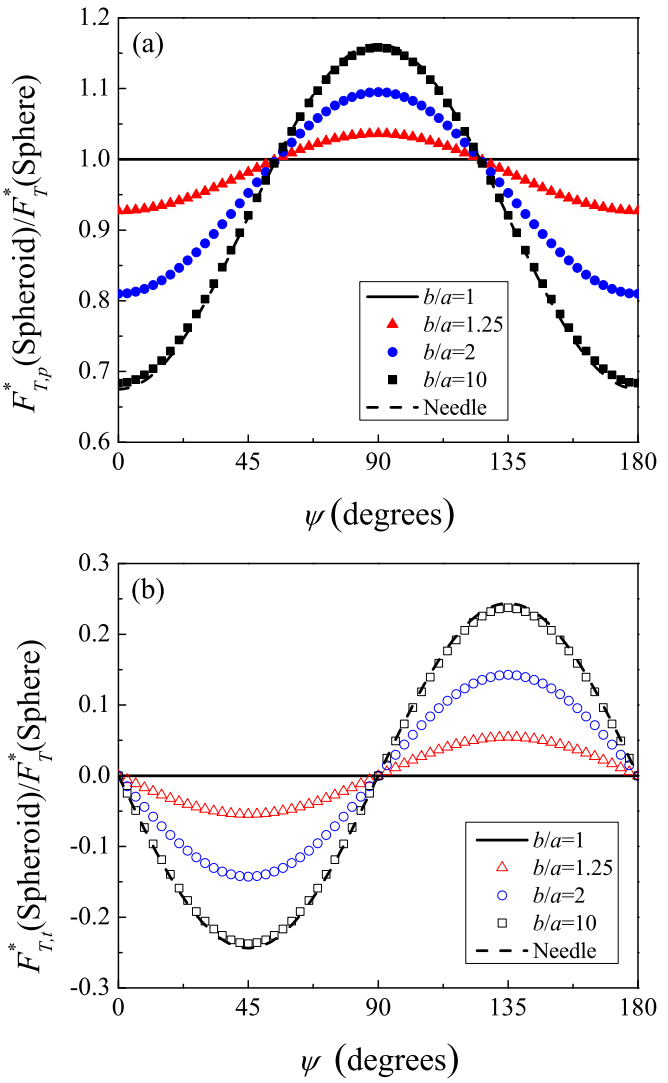

FIG. 5. Variation of the reduced thermophoretic force as a function of ψ for a prolate spheroid: (a) the orientation dependence of the parallel thermophoretic force; (b) the orientation dependence of the transverse force.

where $\mathbf{X}_1 = (X_1, Y_1, Z_1)^{\mathrm{T}}$, and $\mathbf{M}_1$ and $\mathbf{M}_2$ are the transformation matrices from $\{X_1, Y_1, Z_1\}$ to $\{x, y, z\}$ and from $\{X, Y, Z\}$ to $\{X_1, Y_1, Z_1\}$, respectively.

By substituting Eqs. (26) and (27) into Eq. (6), the transformation matrix

$$\mathbf{M} = \mathbf{M}_1 \cdot \mathbf{M}_2. \tag{28}$$

Here, the transformation matrix $\mathbf{M}_1$ is particle shape dependent and independent of the particle orientation, while the transformation matrix $\mathbf{M}_2$ is independent of the particular shape of the particles and depends on the particle orientation.

As shown in Fig. 2(d), a general transformation matrix $\mathbf{M}_1$ can be given by

$$\mathbf{M}_1 = \begin{bmatrix} \sin\phi & 0 & \cos\phi \\ \cos\phi\sin\xi & -\cos\xi & -\sin\phi\sin\xi \\ \cos\phi\cos\xi & \sin\xi & -\sin\phi\cos\xi \end{bmatrix}, \tag{29}$$

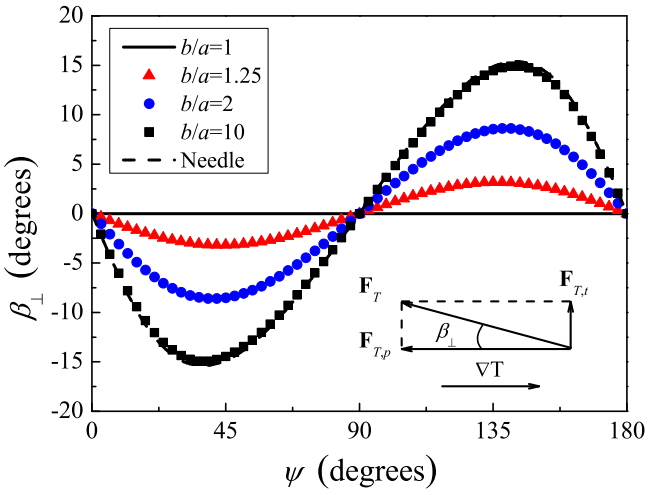

FIG. 6. Orientation dependence of the deviation angle $\beta_\perp$ for a prolate spheroid.

where ϕ denotes the angle between X_1 and the projection of y in the X_1OZ_1 plane and ξ denotes the supplementary angle between y and Y_1. Here, the solid angles (ϕ, ξ) depend on the shape of particles.

For the nonspherical particles, the transformation matrix $\mathbf{M}_2$ can be expressed by the Euler angle (φ, θ, ζ) defined by the three successive rotations, as shown in Figs. 2(a)–2(c). The rotation sequence is as follows:

(a) Rotating the global coordinate system $\{X,Y,Z\}$ by an angle φ clockwise about the Y axis to generate the coordinate system $\{X',Y',Z'\}$ [see Fig. 2(a)].

(b) Rotating the coordinate system $\{X',Y',Z'\}$ by an angle θ clockwise about the Z' axis to generate the coordinate system $\{X'',Y'',Z''\}$ [see Fig. 2(b)].

(c) Rotating the coordinate system $\{X'',Y'',Z''\}$ by an angle ζ clockwise about the Y'' axis to generate the auxiliary coordinate system $\{X_1,Y_1,Z_1\}$ [see Fig. 2(c)].

Therefore,

$$\mathbf{M}_2 = \begin{bmatrix} \cos\zeta\cos\varphi\cos\theta - \sin\zeta\sin\varphi & -\cos\zeta\sin\theta & \cos\zeta\sin\varphi\cos\theta + \sin\zeta\cos\varphi \\ \cos\varphi\sin\theta & \cos\theta & \sin\varphi\sin\theta \\ -\sin\zeta\cos\varphi\cos\theta - \cos\zeta\sin\varphi & \sin\zeta\sin\theta & -\sin\zeta\sin\varphi\cos\theta + \cos\zeta\cos\varphi \end{bmatrix}. \tag{30}$$

Actually, rotation (c) is unnecessary for axisymmetric particles (including, cylinders, spheroids, disks, and needles) if Y_1 is set to be in the direction of the particle axis. The angle between X and Y_1 is denoted by ψ (the angle between the temperature gradient and the axis of particles), and $\cos\psi = \cos\varphi\sin\theta$ (see Fig. 1).

Then, in the following subsections, the thermophoretic forces on several typical nonspherical particles are calculated, including cylinders, spheroids, disks, needles, and cuboids.

C. Cylinders

Consider a cylinder of length L and radius $R_0 (L \gg R_0)$, wherein the end effect of the cylinder can be neglected. As shown in Fig. 3, the solid angles $\xi = 0$ and $0 \leqslant \phi \leqslant 2\pi$. Then, the transformation matrix $\mathbf{M}_1$ for a cylinder

$$\mathbf{M}_{1,\mathrm{cy}} = \begin{bmatrix} \sin\phi & 0 & \cos\phi \\ \cos\phi & 0 & -\sin\phi \\ 0 & 1 & 0 \end{bmatrix}. \tag{31}$$

The surface element

$$dS = R_0 d\phi dY_1. \tag{32}$$

By substituting Eqs. (19)–(22), (28), and (30)–(32) into Eqs. (23)–(25), the instantaneous thermophoretic force components $\{F_X, F_Y, F_Z\}$ on a cylinder can be obtained as follows:

$$F_X = -\frac{\kappa}{5}\sqrt{\frac{2\pi m}{k_B T}} R_0 L \nabla T \left[\sigma_\tau + \left(2 - \sigma_p - \frac{\sigma_\tau}{2}\right)\sin^2\psi\right], \tag{33}$$

$$F_Y = \frac{\kappa}{5}\sqrt{\frac{2\pi m}{k_B T}} \left(2 - \sigma_p - \frac{\sigma_\tau}{2}\right) R_0 L \nabla T \cos\psi\cos\theta, \tag{34}$$

$$F_Z = \frac{\kappa}{5}\sqrt{\frac{2\pi m}{k_B T}} \left(2 - \sigma_p - \frac{\sigma_\tau}{2}\right) R_0 L \nabla T \cos\psi\sin\varphi\sin\theta. \tag{35}$$

Then, the expression for the thermophoretic force on a cylinder in the free-molecule regime is given by

$$\mathbf{F}_T = -\frac{\kappa}{5}\sqrt{\frac{2\pi m}{k_B T}} R_0 L \left[\sigma_\tau \nabla T_\parallel + \left(2 - \sigma_p + \frac{\sigma_\tau}{2}\right)\nabla T_\perp\right], \tag{36}$$

which is consistent with Eq. (2) [45], if $\sigma_t = \sigma_p = \sigma$. Here, the total thermophoretic force are decomposed in the directions parallel and perpendicular to the cylinder axis, respectively, i.e., $\mathbf{F}_T = \mathbf{F}_{T,\parallel} + \mathbf{F}_{T,\perp}$. The thermophoretic force can also be decomposed in the directions parallel and perpendicular to ∇T, $\mathbf{F}_T = \mathbf{F}_{T,p} + \mathbf{F}_{T,t}$. Here, $F_{T,p} = F_{T,\parallel}\cos\psi + F_{T,\perp}\sin\psi$ denotes the thermophoretic force parallel to ∇T (aligned with ∇T), and $F_{T,t} = F_{T,\parallel}\sin\psi - F_{T,\perp}\cos\psi$ denotes the transverse thermophoretic force. Then,

$$F_{T,p} = -\frac{\kappa}{5}\sqrt{\frac{2\pi m}{k_B T}} R_0 L \left[\sigma_\tau \cos^2\psi + \left(2 - \sigma_p + \frac{\sigma_\tau}{2}\right)\sin^2\psi\right]\nabla T, \tag{37}$$

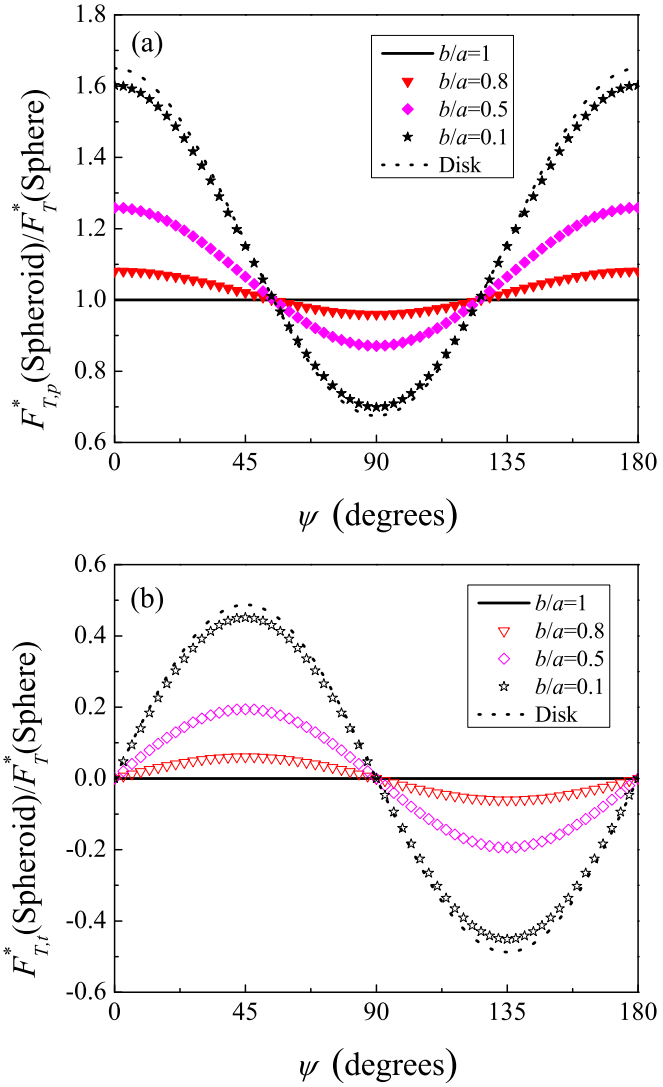

FIG. 7. Variation of the reduced thermophoretic force as a function of ψ for an oblate spheroid: (a) the orientation dependence of the parallel thermophoretic force; (b) the orientation dependence of the transverse force.

$$F_{T,t} = \frac{\kappa}{5}\sqrt{\frac{2\pi m}{k_B T}} R_0 L\left(2 - \sigma_p - \frac{\sigma_\tau}{2}\right)\nabla T \cos\psi \sin\psi. \quad (38)$$

As shown by Eqs. (37) and (38), the total thermophoretic force on the cylinder is not opposite to the direction of temperature gradient ∇T, because a transverse force, $\mathbf{F}_{T,t}$, is induced by the pitching effect of cylinder. In the present paper, the thermophoretic force component opposite to ∇T is called the parallel thermophoretic force, while the component perpendicular to ∇T is called the vertical thermophoretic force or transverse force, for short.

For a small particle undergoing Brownian rotation in the free-molecule regime, it is expected to rotate freely in the absence of a strong external force field [50,55]. Under this assumption, the orientation of the particle undergoes a uniformly random distribution. The average force acting on the particle can be obtained by the orientation averaging,

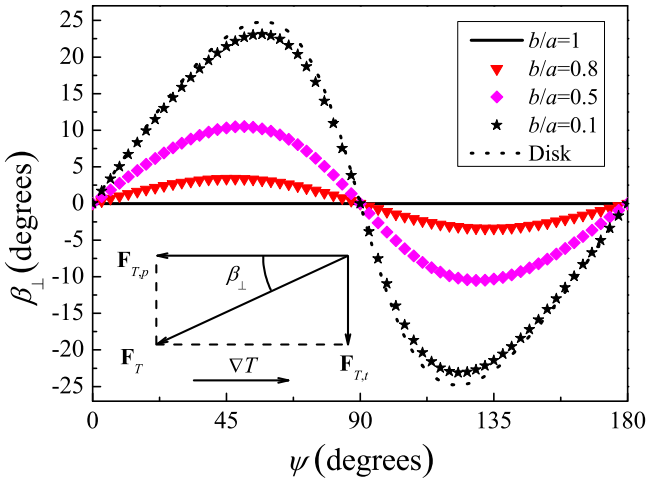

FIG. 8. Orientation dependence of the deviation angle $\beta_\perp$ for an oblate spheroid.

$$\langle F\rangle = \frac{1}{8\pi^2}\int_0^{2\pi}\int_0^{2\pi}\int_0^{\pi} F \sin\theta d\theta d\varphi d\zeta. \quad (39)$$

By substituting Eqs. (33)–(35) into Eq. (39), the transverse force vanishes. Thus, the orientation-averaged thermophoretic force on a cylinder is given by

$$\langle F_T\rangle = -\frac{2\kappa}{15}\sqrt{\frac{2\pi m}{k_B T}}(2 - \sigma_p + \sigma_\tau) R_0 L \nabla T, \quad (40)$$

which is consistent with Wang's result [47] in the rigid-body limit.

D. Spheroids

Consider a spheroid with semiequatorial axis (or radius) a and semipolar axis (or half length) b. As shown in Fig. 4, $0 \leqslant \xi \leqslant \pi$ and $0 \leqslant \phi \leqslant 2\pi$. The transformation matrix $\mathbf{M}_1$ for a spheroid can be expressed as

$$\mathbf{M}_{1,sr} = \begin{bmatrix} \sin\phi & 0 & \cos\phi \\ \cos\phi\sin\xi & -\cos\xi & -\sin\phi\sin\xi \\ \cos\phi\cos\xi & \sin\xi & -\sin\phi\cos\xi \end{bmatrix}. \quad (41)$$

The surface element

$$dS = rd\phi ds = rd\phi\frac{dY_1}{\sin\xi} = aDdY_1 d\phi, \quad (42)$$

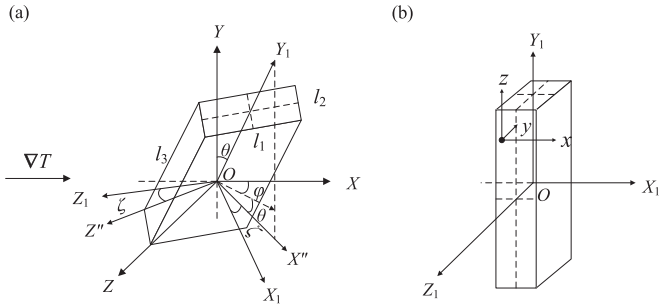

FIG. 9. The coordinate systems for a cuboid.

and the distance between the surface element and the axis

$$r = a\sqrt{1-\frac{Y_1^2}{b^2}} = aD\sin\xi, \tag{43}$$

where

$$D = \sqrt{1+\left(\frac{a^2}{b^2}-1\right)\frac{Y_1^2}{b^2}},$$

$$\sin\xi = \sqrt{1-\frac{Y_1^2}{b^2}}\Big/ D,$$

$$\cos\xi = \frac{a}{b^2}Y_1\Big/ D. \tag{44}$$

By substituting Eqs. (19)–(22), (28), (30), and (41)–(44) into Eqs. (23)–(25), the instantaneous thermophoretic force components $\{F_X, F_Y, F_Z\}$ on the spheroid are given by

$$F_X = -\frac{\kappa}{5}\sqrt{\frac{2\pi m}{k_B T}}a\nabla T\left\{\sigma_\tau\int_{-b}^{b} DdY_1 + \left(2-\sigma_p-\frac{\sigma_\tau}{2}\right)\left[\int_{-b}^{b}\sin^2\xi\, DdY_1 + \cos^2\psi\int_{-b}^{b}(2\cos^2\xi-\sin^2\xi)DdY_1\right]\right\}, \tag{45}$$

$$F_Y = -\frac{\kappa}{5}\sqrt{\frac{2\pi m}{k_B T}}\left(2-\sigma_p-\frac{\sigma_\tau}{2}\right)a\nabla T\cos\psi\cos\theta\int_{-b}^{b}(2\cos^2\xi-\sin^2\xi)DdY_1, \tag{46}$$

$$F_Z = -\frac{\kappa}{5}\sqrt{\frac{2\pi m}{k_B T}}\left(2-\sigma_p-\frac{\sigma_\tau}{2}\right)a\nabla T\cos\psi\sin\varphi\sin\theta\int_{-b}^{b}(2\cos^2\xi-\sin^2\xi)DdY_1. \tag{47}$$

Thus, the thermophoretic force on a spheroid in the free-molecule regime reads

$$\mathbf{F}_T = -\frac{\kappa}{5}\sqrt{\frac{2\pi m}{k_B T}}a\left\{[\sigma_\tau\nabla T_\perp + 2(2-\sigma_p)\nabla T_\parallel]\int_{-b}^{b} DdY_1 + \left(2-\sigma_p-\frac{\sigma_\tau}{2}\right)(\nabla T_\perp - 2\nabla T_\parallel)\int_{-b}^{b}\sin^2\xi\, DdY_1\right\}, \tag{48}$$

where the direction of thermophoretic force also deviates from the opposite direction of ∇T. Being similar to cylinders, the transverse force must vanish after orientation averaging. Thus, the orientation-averaged thermophoretic force

$$\langle F_T\rangle = -\frac{2\kappa}{15}\sqrt{\frac{2\pi m}{k_B T}}(2-\sigma_p+\sigma_\tau)a\nabla T\int_{-b}^{b} DdY_1, \tag{49}$$

which is opposite to ∇T. Note that integral terms in Eqs. (48) and (49) depend on a and b. Then, the explicit expressions for the themophoretic force on spheres, prolate spheroids, and oblate spheroids can be obtained based on Eq. (48), respectively.

1. Sphere ($a = b = R_0$)

For a sphere,

$$\int_{-b}^{b} DdY_1 = 2R_0,$$

$$\int_{-b}^{b}\sin^2\xi\, DdY_1 = \frac{4}{3}R_0. \tag{50}$$

Thus, Eq. (48) becomes

$$\mathbf{F}_T = -\frac{4\kappa}{15}\sqrt{\frac{2\pi m}{k_B T}}(2-\sigma_P+\sigma_\tau)R_0^2\nabla T, \tag{51}$$

which is consistent with Eq. (1), if $\sigma_t = \sigma_p = \sigma$ [36].

2. Prolate spheroid ($b > a$)

For a prolate spheroid,

$$\int_{-b}^{b} DdY_1 = a + \frac{b^2}{\sqrt{b^2-a^2}}\arcsin\frac{\sqrt{b^2-a^2}}{b},$$

$$\int_{-b}^{b}\sin^2\xi\, DdY_1 = \frac{b^2}{b^2-a^2}\left(a + \frac{b^2-2a^2}{\sqrt{b^2-a^2}}\arcsin\frac{\sqrt{b^2-a^2}}{b}\right). \tag{52}$$

If $b/a \gg 1$, the prolate spheroid is like a needle in shape. Then, Eq. (52) can be simplified to

$$\int_{-b}^{b} DdY_1 = \frac{\pi}{2}b,$$
$$\int_{-b}^{b} \sin^2\xi\, DdY_1 = \frac{\pi}{2}b. \tag{53}$$

Thus, the thermophoretic force on the needle is given by

$$\mathbf{F}_T = -\frac{\pi\kappa}{10}\sqrt{\frac{2\pi m}{k_B T}}ab\left[\sigma_\tau \nabla T_\parallel + \left(2 - \sigma_p + \frac{\sigma_\tau}{2}\right)\nabla T_\perp\right]. \tag{54}$$

In this case, the thermophoretic force for an extremely prolate spheroid (a needle) given by Eq. (54) is proportional to that for a cylinder given by Eq. (36) by a coefficient of $\pi/4$ ($a = R_0$, and $b = L/2$).

Figure 5 presents the orientation dependence of the reduced thermophoretic force at different aspect ratios for prolate spheroids. Here, the orientation is denoted by the angle between ∇T (X) and the particle axis (Y_1), ψ. We choose $\sigma_p = \sigma_\tau = 0.9$ for the momentum accommodation coefficients [62]. The reduced thermophoretic forces $F^*_{T,p} = F_{T,p}/S$, $F^*_{T,t} = F_{T,t}/S$, and $F^*_T = F_T/S$ are calculated for spheroids and spheres, respectively. According to Fig. 5(a), the maximum parallel thermophoretic force appears in the case of $\psi = \pi/2$, (i.e., the axis of the spheroid is perpendicular to ∇T), while the minimum is at $\psi = 0$ (i.e., the axis of the spheroid is parallel to ∇T). This is because the gas-particle collision cross section against the temperature gradient decreases from $\psi = \pi/2$ to $\psi = 0$ or $\psi = \pi$, which results in an enhanced momentum transfer at $\psi = \pi/2$. As for the transverse force $F^*_{T,t}$, its magnitude is small compared to the parallel thermophoretic force, but its influence might be significant because it is perpendicular to ∇T. The deviation angle of the total thermophoretic force with respect to $-\nabla T$, $\beta_\perp$, is defined by $\tan\beta_\perp = F_{T,t}/F_{T,p}$, as shown in the inset of Fig. 6, and its maximum is about 15.4°. There is no deviation in the cases of $\psi = 0$ or $\psi = \pi/2$ because of the symmetry. With increasing b/a, the thermophoretic force and the deviation angle for a prolate spheroid vary gently from those for a sphere to a needle.

3. *Oblate spheroid ($a > b$)*

For a oblate spheroid,

$$\int_{-b}^{b} DdY_1 = a + \frac{b^2}{\sqrt{a^2-b^2}}\ln\frac{a+\sqrt{a^2-b^2}}{b},$$
$$\int_{-b}^{b} \sin^2\xi\, DdY_1 = -\frac{b^2}{a^2-b^2}\left(a + \frac{b^2-2a^2}{\sqrt{a^2-b^2}}\ln\frac{a+\sqrt{a^2-b^2}}{b}\right). \tag{55}$$

If $a/b \gg 1$, the oblate spheroid is like a disk in shape. Then, Eq. (55) can be simplified to

$$\int_{-b}^{b} DdY_1 = a,$$
$$\int_{-b}^{b} \sin^2\xi\, DdY_1 = 0. \tag{56}$$

Thus, the thermophoretic force is given by

$$\mathbf{F}_T = -\frac{\kappa}{5}\sqrt{\frac{2\pi m}{k_B T}}a^2[\sigma_\tau \nabla T_\perp + 2(2-\sigma_p)\nabla T_\parallel]. \tag{57}$$

Here, the thermophoretic force on the disk with negligible thickness can also be obtained by the linear superposition of this force on the leading and trailing surfaces.

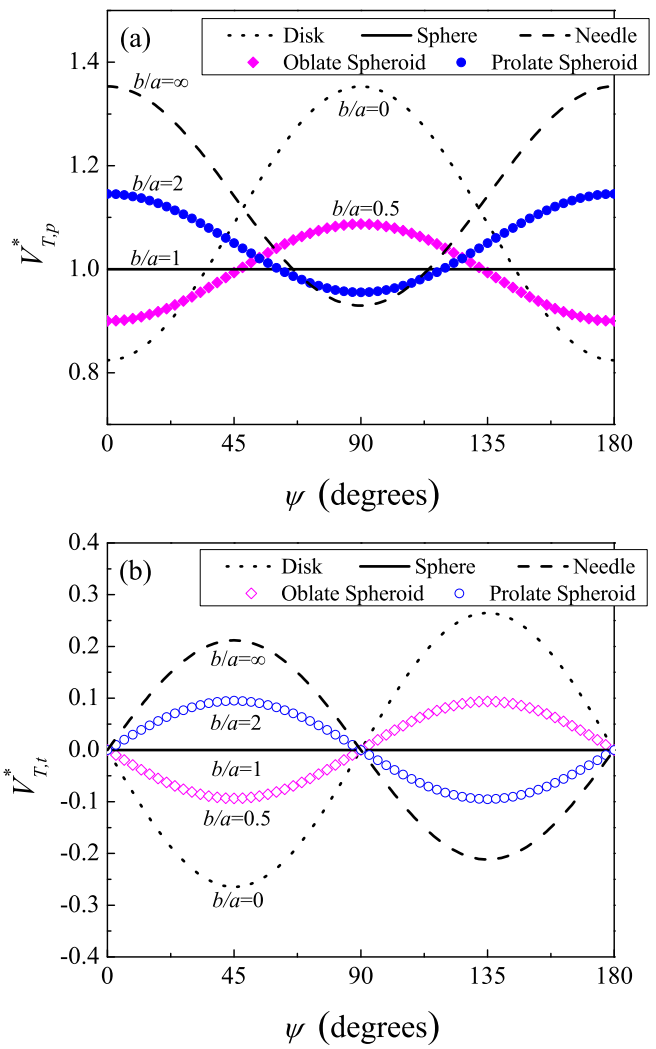

FIG. 10. The reduced thermophoretic velocity versus ψ for nonspheres: (a) the parallel reduced thermophoretic velocities; (b) the transverse reduced thermophoretic velocities.

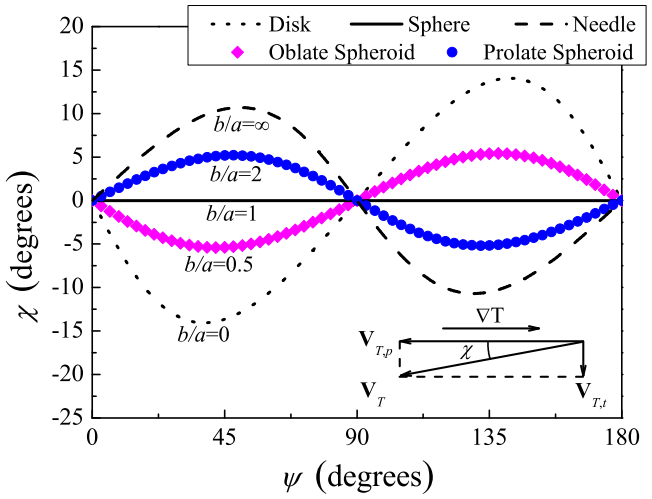

FIG. 11. The deviation angle χ (drift direction with respect to $-\nabla T$) versus ψ for nonspheres.

Figure 7 shows the orientation dependence of the reduced thermophoretic force at different aspect ratios for oblate spheroids. Again, the momentum accommodation coefficients $\sigma_p = \sigma_\tau = 0.9$. It is found that the maximum parallel thermophoretic force appears at $\psi = 0$, while the minimum is at $\psi = \pi/2$ which is different from the prolate spheroids. However, the explanation is in the same manner, i.e., because there is a maximum gas-particle collision cross section against the temperature gradient if the axis is parallel to ∇T. Being similar to the prolate spheroids, the transverse force is small in magnitude and vanishes in the case of $\psi = 0$ or $\psi = \pi/2$. With varying orientation, the magnitude of the reduced transverse force for the oblate spheroid is larger than that for a prolate spheroid, so the influence of the pitching effect is very significant (with a maximum angle around 24.8°; see Fig. 8). The thermophoretic force and the deviation angle for an oblate spheroid are close to those on a disk for very small b/a, and turn into those on a sphere if $b/a = 1$, as it should be.

E. Cuboids

Consider a cuboid with length, width, and height equal to l_1,l_2, and l_3, respectively. The thermophoretic force on the cuboid consists of six parts, i.e., forces on the top, bottom, front, back, left, and right surfaces. It is clear that the rotation angle $\zeta (0 \leqslant \zeta \leqslant 2\pi)$ in Sec. III B has to be considered in the transformation matrix $\mathbf{M}_2$ because a cuboid is not axisymmetric.

In the front surface, the solid angles $\phi = \pi/2$ and $\xi = \pi/2$, as shown in Fig. 9(b). Therefore, the transformation matrix

$$\mathbf{M}_{1,\mathrm{cu}} = \begin{bmatrix} 1 & 0 & 0 \\ 0 & 0 & -1 \\ 0 & 1 & 0 \end{bmatrix}. \tag{58}$$

The surface element

$$dS = dX_1 dY_1. \tag{59}$$

For the other five surfaces, the transformation matrix $\mathbf{M}_1$ can also be obtained in the same way. Finally, the total force is the linear superposition of the forces on these six surfaces,

$$F_X = -\frac{\kappa}{5}\sqrt{\frac{2m}{\pi k_B T}}\sigma_\tau \nabla T(l_1 l_2 + l_2 l_3 + l_3 l_1) - \frac{2\kappa}{5}\sqrt{\frac{2m}{\pi k_B T}}\left(2 - \sigma_p - \frac{\sigma_\tau}{2}\right)\nabla T[l_1 l_2 \cos^2\varphi \sin^2\theta + l_2 l_3(\cos\zeta \sin\varphi + \sin\zeta \cos\varphi \cos\theta)^2 + l_3 l_1(\cos\zeta \cos\varphi \cos\theta - \sin\zeta \sin\varphi)^2], \tag{60}$$

$$F_Y = -\frac{2\kappa}{5}\sqrt{\frac{2m}{\pi k_B T}}\left(2 - \sigma_p - \frac{\sigma_\tau}{2}\right)\nabla T[l_1 l_2 \cos\varphi \sin\theta \cos\theta - l_2 l_3 \sin\zeta \sin\theta(\cos\zeta \sin\varphi + \sin\zeta \cos\varphi \cos\theta) - l_3 l_1 \cos\zeta \sin\theta(\cos\zeta \cos\varphi \cos\theta - \sin\zeta \sin\varphi)], \tag{61}$$

$$F_Z = -\frac{2\kappa}{5}\sqrt{\frac{2m}{\pi k_B T}}\left(2 - \sigma_p - \frac{\sigma_\tau}{2}\right)\nabla T[l_1 l_2 \sin\varphi \cos\varphi \sin^2\theta + l_2 l_3(\sin\zeta \cos\varphi \cos\theta + \cos\zeta \sin\varphi) \times (\sin\zeta \sin\varphi \cos\theta - \cos\zeta \cos\varphi) + l_3 l_1(\cos\zeta \cos\varphi \cos\theta - \sin\zeta \sin\varphi)(\cos\zeta \sin\varphi \cos\theta + \sin\zeta \cos\varphi)]. \tag{62}$$

Then, the total thermophoretic force can be written as

$$\mathbf{F}_T = -\frac{\kappa}{5}\sqrt{\frac{2m}{\pi k_B T}}\{2(2 - \sigma_p)(l_1 l_2 \nabla T_{\perp_1} + l_2 l_3 \nabla T_{\perp_2} + l_3 l_1 \nabla T_{\perp_3}) + \sigma_\tau[(l_2 l_3 + l_3 l_1)\nabla T_{\perp_1} + (l_1 l_2 + l_3 l_1)\nabla T_{\perp_2} + (l_1 l_2 + l_2 l_3)\nabla T_{\perp_3}]\}, \tag{63}$$

and the orientation-averaged thermophoretic force is given by

$$\langle F_T \rangle = -\frac{2\kappa}{15}\sqrt{\frac{2m}{\pi k_B T}}(l_1 l_2 + l_2 l_3 + l_3 l_1)(2 - \sigma_p + \sigma_\tau)\nabla T, \tag{64}$$

where the subscripts "$\perp_1$", "$\perp_2$" and "$\perp_3$" denote that temperature gradient vector is perpendicular to the planes l_1l_2,l_2l_3, and l_3l_1, respectively.

In the case of $l_1 = l_2 = l_3 = l$, the cuboid turns into a cube, and the thermophoretic force is given by

$$\mathbf{F}_T = -\frac{2\kappa}{5}\sqrt{\frac{2m}{\pi k_B T}}(2 - \sigma_p + \sigma_\tau)l^2\nabla T. \tag{65}$$

Note that the thermophoretic force on a cube is exactly in the direction opposite to the temperature gradient; i.e., there is no transverse force for a cube.

F. Thermophoretic velocity

As mentioned in Sec. I, the balance between the thermophoretic and drag forces results in a thermophoretic velocity. For a nonspherical particle, it has been shown that the thermophoretic force is not aligned with the temperature gradient ∇T, and there is a transverse force due to the pitching effect. Therefore, the thermophoretic velocity of the nonspherical particle is supposed to deviate from the negative direction of ∇T. Following Ref. [36], the expression for thermophoretic velocity is obtained by balancing the thermophoretic force with the drag force (see Appendix), i.e., $\mathbf{F}_D + \mathbf{F}_T = 0$.

For cylinders, the thermophoretic velocity components parallel and perpendicular to the cylinder axis are given by

$$V_{T,\parallel} = -\frac{\kappa\nabla T_\parallel}{5nk_BT}, \tag{66}$$

$$V_{T,\perp} = -\frac{\kappa\nabla T_\perp}{5nk_BT}\left(\frac{8 - 4\sigma_p + 2\sigma_\tau}{8 - 4\sigma_p + \pi\sigma_p + 2\sigma_\tau}\right), \tag{67}$$

which is consistent with Ref. [47] if $\sigma_t = \sigma_p = \sigma$. It is found that the thermophoretic velocity is independent of the cylinder size. To clearly illustrate the influence of the particle shape on its thermophoretic motion under a temperature gradient, Eqs. (66) and (67) are rewritten in the directions parallel and perpendicular to ∇T, i.e., $V_{T,p}$ and $V_{T,t}$,

$$V_{T,p} = -\frac{\kappa}{5nk_BT}\left(\cos^2\psi + \frac{8 - 4\sigma_p + 2\sigma_\tau}{8 - 4\sigma_p + \pi\sigma_p + 2\sigma_\tau}\sin^2\psi\right)\nabla T, \tag{68}$$

$$V_{T,t} = -\frac{\kappa}{5nk_BT}\left(\frac{\pi\sigma_p}{8 - 4\sigma_p + \pi\sigma_p + 2\sigma_\tau}\right)\nabla T\sin\psi\cos\psi. \tag{69}$$

For spheroids, the thermophoretic velocity components parallel and perpendicular to the axis can be obtained as

$$V_{T,\parallel} = -\frac{\kappa\nabla T_\parallel}{5nk_BT}\left[\frac{4(2 - \sigma_p)\int_{-b}^{b}\cos^2\xi\, DdY_1 + 2\sigma_\tau\int_{-b}^{b}\sin^2\xi\, DdY_1}{(8 - 4\sigma_p + \pi\sigma_p)\int_{-b}^{b}\cos^2\xi\, DdY_1 + 2\sigma_\tau\int_{-b}^{b}\sin^2\xi\, DdY_1}\right], \tag{70}$$

$$V_{T,\perp} = -\frac{\kappa\nabla T_\perp}{5nk_BT}\left[\frac{4\sigma_\tau\int_{-b}^{b}\cos^2\xi\, DdY_1 + (8 - 4\sigma_p + 2\sigma_\tau)\int_{-b}^{b}\sin^2\xi\, DdY_1}{4\sigma_\tau\int_{-b}^{b}\cos^2\xi\, DdY_1 + (8 - 4\sigma_p + \pi\sigma_p + 2\sigma_\tau)\int_{-b}^{b}\sin^2\xi\, DdY_1}\right]. \tag{71}$$

The thermophoretic velocity components parallel and perpendicular to ∇T are given by

$$V_{T,p} = -\frac{\kappa}{5nk_BT}\left[\frac{4(2 - \sigma_p) - (8 - 4\sigma_p - 2\sigma_\tau)\Gamma}{(8 - 4\sigma_p + \pi\sigma_p) - (8 - 4\sigma_p + \pi\sigma_p - 2\sigma_\tau)\Gamma}\cos^2\psi + \frac{4\sigma_\tau + (8 - 4\sigma_p - 2\sigma_\tau)\Gamma}{4\sigma_\tau + (8 - 4\sigma_p + \pi\sigma_p - 2\sigma_\tau)\Gamma}\sin^2\psi\right]\nabla T, \tag{72}$$

$$V_{T,t} = -\frac{\kappa}{5nk_BT}\left[\frac{4(2 - \sigma_p) - (8 - 4\sigma_p - 2\sigma_\tau)\Gamma}{(8 - 4\sigma_p + \pi\sigma_p) - (8 - 4\sigma_p + \pi\sigma_p - 2\sigma_\tau)\Gamma} - \frac{4\sigma_\tau + (8 - 4\sigma_p - 2\sigma_\tau)\Gamma}{4\sigma_\tau + (8 - 4\sigma_p + \pi\sigma_p - 2\sigma_\tau)\Gamma}\right]\nabla T\sin\psi\cos\psi, \tag{73}$$

respectively. Here, $\Gamma = \int_{-b}^{b}\sin^2\xi\, DdY_1/\int_{-b}^{b} DdY_1$, and other integrals in Eqs. (70)–(73) have been given in Sec. III D.

Figure 10(a) presents the orientation dependence of the reduced thermophoretic velocities for spheres, spheroids, needles, and disks. Here, the reduced thermophoretic velocity is defined as $V_T^* = V_T/V_{T,\text{sphere}}$, where $V_{T,\text{sphere}}$ is the thermophoretic velocity

for spheres,

$$V_{T,\text{sphere}} = -\frac{4(2-\sigma_p+\sigma_\tau)\kappa\nabla T}{5(8-4\sigma_p+\pi\sigma_p+4\sigma_\tau)nk_BT}. \tag{74}$$

The momentum accommodation coefficients $\sigma_p = \sigma_\tau = 0.9$. For spheres, the reduced parallel thermophoretic velocity component $V^*_{T,p}$ is equal to unit and the reduced transverse component $V^*_{T,t}$ is zero. For nonspheres, $V^*_{T,p}$ is unambiguously orientation dependent, while $V^*_{T,t}$ is small in magnitude and is expected to vanish after orientation averaging. At $\psi = 0$ (with the particle axis aligned with ∇T), $V^*_{T,p}$ of a prolate spheroid (including a needle) is larger than unit (by 35.3% for a needle), and $V^*_{T,p}$ of an oblate spheroid (including a disk) is less than unit (by 17.6% for a disk) because of the suppressed (enhanced) friction on a prolate (oblate) spheroid when the axis is aligned with its moving direction. At $\psi = \pi/2$ (with the particle axis perpendicular to ∇T), the parallel thermophoretic velocity of a prolate particle is less than that of an oblate particle. Figure 11 plots the deviation angle of the thermophoretic velocity with respect to $-\nabla T$ (see the inset in Fig. 11). The maximal deviation angle is as high as 14° for a disk at about $\psi = \pi/4$, which highlights the influence of the particle shape on the thermophoretic motion because the moving direction can be changed by the transverse forces.

For cuboids, the thermophoretic velocity components read

$$V_{T,\perp_1} = -\frac{\kappa\nabla T_{\perp_1}}{5nk_BT}\left[\frac{4(2-\sigma_p)l_1l_2+2\sigma_\tau(l_2l_3+l_3l_1)}{(8-4\sigma_p+\pi\sigma_p)l_1l_2+2\sigma_\tau(l_2l_3+l_3l_1)}\right], \tag{75}$$

$$V_{T,\perp_2} = -\frac{\kappa\nabla T_{\perp_2}}{5nk_BT}\left[\frac{4(2-\sigma_p)l_2l_3+2\sigma_\tau(l_1l_2+l_3l_1)}{(8-4\sigma_p+\pi\sigma_p)l_2l_3+2\sigma_\tau(l_1l_2+l_3l_1)}\right], \tag{76}$$

$$V_{T,\perp_3} = -\frac{\kappa\nabla T_{\perp_3}}{5nk_BT}\left[\frac{4(2-\sigma_p)l_3l_1+2\sigma_\tau(l_1l_2+l_2l_3)}{(8-4\sigma_p+\pi\sigma_p)l_3l_1+2\sigma_\tau(l_1l_2+l_2l_3)}\right]. \tag{77}$$

Here, the thermophoretic velocity is size dependent. In the case of $l_1 = l_2 = l_3 = l$, the cuboid turns into a cube. Its thermophoretic velocity is size independent and reads

$$V_T = -\frac{4(2-\sigma_p+\sigma_\tau)\kappa\nabla T}{5(8-4\sigma_p+\pi\sigma_p+4\sigma_\tau)nk_BT}. \tag{78}$$

G. Thermophoretic torque

For a general particle orientation with angle (φ, θ, ζ), the thermophoretic torque $\mathbf{T}$ on the particle can be calculated by integration of the torque $d\mathbf{T}$ on the surface element dS over the whole particle surface,

$$\mathbf{T} = \int_S d\mathbf{T} = \int_S (\mathbf{r}\times\boldsymbol{\tau}_x + \mathbf{r}\times\mathbf{p} + \mathbf{r}\times\boldsymbol{\tau}_z)dS, \tag{79}$$

where $\mathbf{p}$, $\boldsymbol{\tau}_x$, and $\boldsymbol{\tau}_z$ are the normal and tangential forces and $\mathbf{r} = r_{X_1}\mathbf{I}_1 + r_{Y_1}\mathbf{J}_1 + r_{Z_1}\mathbf{K}_1$ the position vector from the mass center of the particle to the surface element.

For the cylinder, the thermophoretic torque components $\{T_{X_1}, T_{Y_1}, T_{Z_1}\}$ are given by

$$T_{X_1} = \int_{-L/2}^{L/2}\int_0^{2\pi}(Y_1\tau_x\cos\phi - Y_1 p\sin\phi - R_0\tau_z\sin\phi)R_0 d\phi dY_1 = 0, \tag{80}$$

$$T_{Y_1} = \int_{-L/2}^{L/2}\int_0^{2\pi}\tau_x R_0^2 d\phi dY_1 = 0, \tag{81}$$

$$T_{Z_1} = \int_{-L/2}^{L/2}\int_0^{2\pi}(-Y_1\tau_x\sin\phi - Y_1 p\cos\phi - R_0\tau_z\cos\phi)R_0 d\phi dY_1 = 0, \tag{82}$$

which is consistent with results of Ref. [45].

For the spheroid, the thermophoretic torque components read

$$T_{X1} = \int_{-b}^{b}\int_{0}^{2\pi} (Y_1\tau_x \cos\phi + rp\cos\xi\sin\phi - Y_1 p\sin\xi\sin\phi - r\tau_z \sin\xi\sin\phi - Y_1\tau_z\cos\xi\sin\phi)aDd\phi dY_1 = 0, \quad (83)$$

$$T_{Y_1} = \int_{-b}^{b}\int_{0}^{2\pi} \tau_x raDd\phi dY_1 = 0, \quad (84)$$

$$T_{Z1} = \int_{-b}^{b}\int_{0}^{2\pi} (-Y_1\tau_x \sin\phi + rp\cos\xi\cos\phi - Y_1 p\sin\xi\cos\phi - r\tau_z \sin\xi\cos\phi - Y_1\tau_z\cos\xi\cos\phi)aDd\phi dY_1 = 0, \quad (85)$$

where, r, $\sin\xi$, $\cos\xi$, and D are given in Eqs. (43) and (44).

For the cuboid, the thermophoretic torque components $\{T_{X_1}, T_{Y_1}, T_{Z_1}\}$ on the front surface (see Fig. 9) can be written as

$$T_{X_1,f} = \int_{-l_3/2}^{l_3/2}\int_{-l_2/2}^{l_2/2}\left(-Yp - \frac{l_1}{2}\tau_z\right)dX_1dY_1 = \frac{\kappa}{10}\sqrt{\frac{m}{2\pi k_B T}}l_1 l_2 l_3 \nabla T\cos\varphi\sin\theta, \quad (86)$$

$$T_{Y_1,f} = \int_{-l_3/2}^{l_3/2}\int_{-l_2/2}^{l_2/2}\left(\frac{l_1}{2}\tau_x + X_1 p\right)dX_1dY_1 = -\frac{\kappa}{10}\sqrt{\frac{m}{2\pi k_B T}}l_1 l_2 l_3 \nabla T(\cos\zeta\cos\varphi\cos\theta - \sin\zeta\sin\varphi), \quad (87)$$

$$T_{Z_1,f} = \int_{-l_3/2}^{l_3/2}\int_{-l_2/2}^{l_2/2}(-Y_1\tau_x + X_1\tau_z)dX_1dY_1 = 0. \quad (88)$$

In the back surface, both x and y directions are reversed, and the thermophoretic torque components read

$$T_{X_1,b} = \int_{-l_3/2}^{l_3/2}\int_{-l_2/2}^{l_2/2}\left(Yp + \frac{l_1}{2}\tau_z\right)dX_1dY_1 = -\frac{\kappa}{10}\sqrt{\frac{m}{2\pi k_B T}}l_1 l_2 l_3 \nabla T\cos\varphi\sin\theta, \quad (89)$$

$$T_{Y_1,b} = \int_{-l_3/2}^{l_3/2}\int_{-l_2/2}^{l_2/2}\left(\frac{l_1}{2}\tau_x - X_1 p\right)dX_1dY_1 = \frac{\kappa}{10}\sqrt{\frac{m}{2\pi k_B T}}l_1 l_2 l_3 \nabla T(\cos\zeta\cos\varphi\cos\theta - \sin\zeta\sin\varphi), \quad (90)$$

$$T_{Z_1,b} = \int_{-l_3/2}^{l_3/2}\int_{-l_2/2}^{l_2/2}(-Y_1\tau_x + X_1\tau_z)dX_1dY_1 = 0, \quad (91)$$

which can be counteracted by the thermophoretic torques on the front surface. Similarly, the thermophoretic torques for the other four surfaces counteract each other due to the symmetry. Finally, the cuboid experiences zero net thermophoretic torque.

According to the above calculations, there is no net thermophoretic torque on cylinders, spheroids, and cuboids, which can be attributed to the symmetry of their particular shape. In fact, it has been reported that any particle that has three mutually perpendicular planes of symmetry will experience zero net thermophoretic torque [45].

IV. CONCLUSION

In summary, we have theoretically studied the thermophoresis of the nonspherical rigid particles in the free-molecule regime based on the gas kinetic theory. The formulas for the thermophoretic forces acting on the convex particles, especially several typical nonspherical bodies, including cylinders, spheroids, needles, disks, and cuboids, are obtained by considering the influence of the particle shape and orientation. The expressions for the thermophoretic forces on the cylinders and spheres (a special case of spheroids) are consistent with those in the open literature. Due to the pitching effect of nonspheres, there exist transverse forces perpendicular to the temperature gradient, which might significantly affect the thermophoresis (especially its direction) of nonspherical particles even though it is small in magnitude compared to the force component opposite to the temperature gradient. Under a uniformly random distribution of the particle orientation, the expressions for the orientation-averaged thermophoretic forces are obtained by orientation averaging.

ACKNOWLEDGMENT

This work is supported by the National Natural Science Foundation of China (Grant No. 51776007).

APPENDIX

A particle suspended in a gas with a nonuniform temperature distribution is subjected to a thermophoretic force as well as a drag. In the steady state, the particle moves with a thermophoretic velocity by balancing the thermophoretic force with the drag force on the particle. The normal and tangential drag forces on the surface element are

given by

$$p_i = \frac{\rho}{2\sqrt{\pi}h^2}\left\{hv_0\exp\left(-h^2v_0^2\right)+\sqrt{\pi}\left(h^2v_0^2+\frac{1}{2}\right)[1+\mathrm{erf}(hv_0)]\right\}, \tag{A1}$$

$$\tau_{xi} = \frac{\rho u_0}{2\sqrt{\pi}h}\left\{\exp\left(-h^2v_0^2\right)+\sqrt{\pi}hv_0[1+\mathrm{erf}(hv_0)]\right\}, \tag{A2}$$

$$\tau_{zi} = \frac{\rho w_0}{2\sqrt{\pi}h}\left\{\exp\left(-h^2v_0^2\right)+\sqrt{\pi}hv_0[1+\mathrm{erf}(hv_0)]\right\}, \tag{A3}$$

$$p_w = \frac{\rho}{4h^2}\left\{\exp\left(-h^2v_0^2\right)+\sqrt{\pi}hv_0[1+\mathrm{erf}(hv_0)]\right\}, \tag{A4}$$

where $\mathrm{erf}(x) = (2/\sqrt{\pi})\int_0^x e^{-\eta^2}d\eta$ is the error function. Thus, the drag force on a cylinder is given by

$$\mathbf{F}_D = -n\sqrt{2\pi mk_BT}R_0L\left[\sigma_\tau\mathbf{V}_\parallel+\left(2-\sigma_p+\frac{\pi}{4}\sigma_p+\frac{\sigma_\tau}{2}\right)\mathbf{V}_\perp\right]. \tag{A5}$$

The drag force on a spheroid reads

$$\mathbf{F}_D = -n\sqrt{2\pi mk_BT}a\left\{\left[\sigma_\tau\mathbf{V}_\perp+2\left(2-\sigma_p+\frac{\pi}{4}\sigma_p\right)\mathbf{V}_\parallel\right]\int_{-b}^{b}DdY_1+\left(2-\sigma_p+\frac{\pi}{4}\sigma_p-\frac{\sigma_\tau}{2}\right)(\mathbf{V}_\perp-2\mathbf{V}_\parallel)\int_{-b}^{b}\sin^2\xi DdY_1\right\}, \tag{A6}$$

and the drag force on a cuboid can be written as

$$\mathbf{F}_D = -n\sqrt{\frac{2mk_BT}{\pi}}\left\{2\left(2-\sigma_p+\frac{\pi}{4}\sigma_p\right)\left(l_1l_2\mathbf{V}_{\perp_1}+l_2l_3\mathbf{V}_{\perp_2}+l_3l_1\mathbf{V}_{\perp_3}\right)+\sigma_\tau\left[(l_2l_3+l_3l_1)\mathbf{V}_{\perp_1}+(l_1l_2+l_3l_1)\mathbf{V}_{\perp_2}+(l_1l_2+l_2l_3)\mathbf{V}_{\perp_3}\right]\right\}. \tag{A7}$$

The above results are consistent with the drag expressions given in Ref. [62] if we assume that $\sigma_\tau = \sigma_p$.

[1] C. N. Davies, *Aerosol Science* (Academic, New York, 1966).
[2] L. Waldmann and K. H. Schmitt, *Thermophoresis and Diffusiophoresis of Aerosol* (Academic Press, New York, 1966).
[3] B. V. Derjaguin and Y. I. Yalamov, *The Theory of Thermophoresis and Diffusiophoresis of Aerosol Particles and Their Experimental Testing* (Pergamon Press, Oxford, 1972).
[4] F. Zheng, Adv. Colloid Interface Sci. **97**, 255 (2002).
[5] B. H. Kaye, *Direct Characterization of Fine Particles* (Wiley, New York, 1981).
[6] B. Bai, X. Li, and S. Li, AIAA J. **54**, 2069 (2016).
[7] Y. Ye, D. Y. H. Pui, B. Y. H. Liu, S. Opiolka, S. Blumhorst, and H. Fissan, J. Aerosol Sci. **22**, 63 (1991).
[8] S. K. Friedlander and D. Smoke, *Haze: Fundamentals of Aerosol Dynamics* (Oxford University Press, New York, 2000).
[9] S. K. Friedlander, J. F. De La Mora, and S. A. Gokoglu, J. Colloid Interface Sci. **125**, 351 (1988).
[10] S. A. Gokoglu and D. E. Rosner, Chem. Eng. Commun. **44**, 107 (1986).
[11] M. M. R. Williams and S. K. Loyalka, *Aerosol Science: Theory and Practice, With Special Applications to the Nuclear Industry* (Pergamon Press, New York, 1991).
[12] D. E. Rosner, D. W. Mackowski, and P. Garcia-Ybarra, Combust. Sci. Technol. **80**, 87 (1991).
[13] Z. A. Gomez and D. E. Rosner, Combust. Sci. Technol. **89**, 335 (1993).
[14] A. Messerer, R. Niessner, and U. Pöschl, Aerosol Sci. Technol. **38**, 456 (2004).
[15] Z. Xu and H. Zhao, Combust. Flame **162**, 2200 (2015).
[16] N. J. Kempema and M. B. Long, Combust. Flame **164**, 373 (2016).
[17] Y. Sone and K. Aoki, in *Rarefied Gas Dynamics*, edited by S. Fisher (AIAA, New York, 1981), p. 489.
[18] Z. Li and H. Wang, Phys. Rev. E **70**, 021205 (2004).
[19] T. Ohwada and Y. Sone, Eur. J. Mech. B-Fluids **11**, 389 (1992).
[20] J. Wang and Z. Li, Phys. Rev. E **84**, 021201 (2011).
[21] J. Wang and Z. Li, Phys. Rev. E **86**, 011201 (2012).
[22] S. Duhr and D. Braun, Proc. Natl. Acad. Sci. USA **103**, 19678 (2006).
[23] R. W. Bosworth, A. L. Ventura, A. D. Ketsdever, and S. F. Gimelshein, J. Fluid Mech. **805**, 207 (2016).
[24] T. Tsuji, H. Iseki, I. Hanasaki, and S. Kawano, J. Phys.: Condens. Matter **29**, 475101 (2017).
[25] P. S. Epstein, Z. Phys. **54**, 537 (1929).
[26] J. R. Brock, J. Colloid Sci. **17**, 768 (1962).
[27] Y. Sone and K. Aoki, in *Rarefied Gas Dynamics*, edited by J. L. Potter (AIAA, New York, 1977), p. 417.
[28] K. Yamamoto and Y. Ishihara, Phys. Fluids **31**, 3618 (1988).
[29] S. K. Loyalka, J. Aerosol Sci. **23**, 291 (1992).
[30] S. Takata, K. Aoki, and Y. Sone, in *Rarefied Gas Dynamics*, edited by B. D. Shizgal and D. P. Weaver (AIAA, New York, 1994), p. 626.
[31] E. Bringuier and A. Bourdon, Physica A **385**, 9 (2007).
[32] S. R. de Groot and P. Mazur, *Non-equilibrium Thermodynamics* (North-Holland, Amsterdam, 1969).
[33] M. E. Schimpf and S. N. Semenov, J. Phys. Chem. B **104**, 9935 (2000).

[34] G. A. Bird, *Molecular Gas Dynamics and the Direct Simulation of Gas Flows* (Oxford University Press, New York, 1994).
[35] S. Chapman and T. G. Cowling, *The Mathematical Theory of Non-Uniform Gases* (Cambridge University Press, Cambridge, 1970).
[36] L. Waldmann, Z. Naturforsch., A: Phys. Sci. **14**, 589 (1959).
[37] C. F. Schadt and R. D. Cadle, J. Phys. Chem. **65**, 1689 (1961).
[38] S. Jacobsen and J. R. Brock, J. Colloid Sci. **20**, 544 (1965).
[39] L. A. Davis and T. W. Adair III, J. Chem. Phys. **62**, 2278 (1975).
[40] N. T. Tong, J. Colloid Interface Sci. **51**, 143 (1975).
[41] F. Prodi, G. Santachiara, and V. Prodi, J. Aerosol Sci. **10**, 421 (1979).
[42] W. Li and E. J. Davis, J. Aerosol Sci. **26**, 1063 (1995).
[43] W. Li and E. J. Davis, J. Aerosol Sci. **26**, 1085 (1995).
[44] S. Beresnev and V. Chernyak, Phys. Fluids **7**, 1743 (1995).
[45] P. Garcia-Ybarra and D. E. Rosner, AIChE J. **35**, 139 (1989).
[46] X. Chen, J. Phys. D: Appl. Phys. **33**, 803 (2000).
[47] J. Wang, S. Luo, and G. Xia, Phys. Rev. E **95**, 033101 (2017).
[48] Y. Zhang, S. Li, W. Yan, and Q. Yao, Powder Technol. **227**, 24 (2012).
[49] P. Laiho, K. Mustonen, Y. Ohno, S. Maruyama, and E. I. Kauppinen, ACS Appl. Mater. Interfaces **9**, 20738 (2017).
[50] M. Li, G. W. Mulholland, and M. R. Zachariah, Aerosol Sci. Technol. **46**, 1035 (2012).
[51] M. Li, R. You, G. W. Mulholland, and M. R. Zachariah, Aerosol Sci. Technol. **48**, 22 (2014).
[52] M. Li, G. W. Mulholland, and M. R. Zachariah, Phys. Rev. E **89**, 022112 (2014).
[53] R. Y. M. Wong, C. Liu, J. Wang, C. Y. H. Chao, and Z. Li, J. Nanosci. Nanotechnol. **12**, 2311 (2012).
[54] C. Liu, R. Zhao, R. Xu, F. N. Egolfopoulos, and H. Wang, Proc. Combust. Inst. **36**, 1523 (2017).
[55] C. Liu, Z. Li, and H. Wang, Phys. Rev. E **94**, 023102 (2016).
[56] K. Chae and A. Violi, J. Chem. Phys. **134**, 044537 (2011).
[57] L. Yang, J. Feng, Y. Ding, J. Bian, and G. Wang, AIP Adv. **6**, 085113 (2016).
[58] B. Y. Cao and R. Y. Dong, J. Chem. Phys. **140**, 034703 (2014).
[59] R. Y. Dong and B. Y. Cao, Sci. Rep. **4**, 6120 (2014).
[60] R. Y. Dong and B. Y. Cao, RSC Adv. **5**, 88719 (2015).
[61] K. Wang and H. Zhao, Aerosol Sci. Technol. **49**, 75 (2015).
[62] B. E. Dahneke, J. Aerosol Sci. **4**, 147 (1973).
[63] N. Liu and D. B. Bogy, Phys. Fluids **20**, 107102 (2008).
[64] N. Liu and D. B. Bogy, Phys. Fluids **21**, 047102 (2009).